Nano Research 2018, 11(3): 1294–1300
https://doi.org/10.1007/s12274-017-1743-8
Research Article

ISSN 1998-0124
CN 11-5974/O4

Three-dimensional interconnected Ni(Fe)O_xH_y nanosheets on stainless steel mesh as a robust integrated oxygen evolution electrode

Qi Zhang[1,2], Haixia Zhong[2], Fanlu Meng[2], Di Bao[2], Xinbo Zhang[2], and Xiaolin Wei[1] (✉)

[1] *Hunan Key Laboratory for Micro-Nano Energy Materials and Device, Department of Physics, Xiangtan University, Xiangtan 411105, China*

[2] *State Key Laboratory of Rare Earth Resource Utilization, Changchun Institute of Applied Chemistry, Chinese Academy of Sciences, Changchun 130022, China*

Received: 20 April 2017
Revised: 22 June 2017
Accepted: 24 June 2017

KEYWORDS

oxygen evolution reaction, three-dimensional (3D) architecture, stainless steel mesh (SSNNi), integrated oxygen evolution electrode

ABSTRACT

The development of an electrocatalyst based on abundant elements for the oxygen evolution reaction (OER) is important for water splitting associated with renewable energy sources. In this study, we develop an interconnected Ni(Fe)O_xH_y nanosheet array on a stainless steel mesh (SSNNi) as an integrated OER electrode, without using any polymer binder. Benefiting from the well-defined three-dimensional (3D) architecture with highly exposed surface area, intimate contact between the active species and conductive substrate improved electron and mass transport capacity, facilitated electrolyte penetration, and improved mechanical stability. The SSNNi electrode also has excellent OER performance, including low overpotential, a small Tafel slope, and long-term durability in the alkaline electrolyte, making it one of the most promising OER electrodes developed.

1 Introduction

With aspirations to alleviate the rising global energy and ecological crisis due to the enormous consumption of fossil fuels, extensive research has been conducted in the field of clean, renewable energy sources, and in the development of more efficient energy conversion and storage techniques [1–4]. Among many approaches, electrochemically splitting water into hydrogen and oxygen at high purity and low cost, especially if coupled with a renewable energy system (ie. solar or wind), is widely believed to be a promising way to address the above issues [5–7]. However, the anodic oxygen evolution reaction (OER) involves complex proton-coupling steps, limiting the overall efficiency of these devices, which require

Address correspondence to to xlw@xtu.edu.cn

extremely efficient catalysts to accelerate the reaction [8, 9]. Currently, noble metal based materials, such as RuO_2 and IrO_2, represent the benchmark for OER catalysts. However, these materials suffer from some problems, including their high cost, scarcity, and limited stability, severely impeding their practical application on a large scale [10, 11]. Therefore, there is an urgent need to develop efficient and durable catalysts based on abundantly available metals to expedite the reaction, reduce the overpotential, and increase overall energy efficiency.

To date, tremendous progress has been made in developing transition metal based catalysts (such as metal oxides/hydroxides, phosphides, chalcogenides, and nitrides), which present promising alternatives due to their low-cost and considerable OER catalytic activities [12–19]. However, their inferior catalytic activities compared to the noble metal based catalysts have imposed restrictions on their commercial application. This can likely be attributed to slow electron-transfer kinetics during the catalytic process caused by the intrinsically high electrical resistance of many transition metals [20, 21]. A promising way to improve the OER performance is to support these catalysts on conductive substrates. These electrodes are conventionally prepared by dip-casting or spin-casting the catalysts onto two-dimensional (2D) planar substrates, using a polymer binder (polytetrafluoroethylene (PTFE), Nafion, etc.) to immobilize them, which is complicated and costly. Additionally, these binders inevitably lead to covered active sites, insufficient contact between the active sites and the substrate, and accumulation of gases on the planar substrates. These gases tend to block the mass and electron transport, and cause a deterioration in catalytic activity [22, 23]. Moreover, they suffer from poor stability during the OER process, since the catalyst easily peels off from the substrate under continuous O_2 evolution/bubbling [24, 25]. Therefore, it is critically important to build an economical OER electrode with optimized architecture for effective catalytic activity and long-term durability.

Recently, well-defined three-dimensional (3D) architecture OER electrodes have emerged as excellent candidates due to their large amount of exposed surface area, intimate connections between the active sites and current collector, easy electrolyte penetration, high conductivity, and mechanical stability [26–30]. Remarkably, a stainless steel mesh (SS) can be not only used as the current collector or structure scaffold, but also as the active species source, because it contains active elements such as Fe, Ni, and Mn. However, SS protected with anticorrosive layers cannot be directly used as an OER electrode, since these layers are inactive. To address this issue, removal of the anticorrosive film and *in-situ* construction of the active material array on the whole skeleton of SS provides a possible stratagem to boost the OER performance. Ni(Fe) oxides or hydroxides can be directly grown on SS using a specific corroding process, and are considered to be the most active OER catalysts [9, 28, 31]. Thus, constructing a 3D integrated electrode and incorporating a Ni(Fe) species array to expedite the reaction is technologically important and urgently needed.

With these considerations in mind, we developed hierarchical cross-linked Ni(Fe) hydroxide nanosheet arrays on SS (SSNNi), using the hydrothermal method. The interconnected hierarchical nanosheet arrays are continuously and closely grown across the whole SSNNi structure, ensuring fast electron and mass transport. Moreover, the SSNNi electrode can be directly used as a robust OER electrode without using any polymer binder, owing to the close contact between the active sites and current collector, high exposed active surface area, enhanced electron and mass transport, and stable structure. As expected, SSNNi exhibits excellent OER performance with low overpotential, a small Tafel slope, and long-term durability in the alkaline electrolyte.

2 Experimental

The facile and scalable fabrication process of the 3D integrated SSNNi electrode is schematically shown in Fig. 1. First, the SS was washed with water and ethanol to remove any impurities. Then, the SS was immersed into an aqueous solution containing NH_4HCO_3 and $NiCl_2$, and sealed in an autoclave. Then, it was heated at 100 ˚C for 8 h. For comparison, SS with hydrothermal treatment in NH_4HCO_3 and $NiCl_2$ solution alone was also produced and designated as SSN or SSNi, respectively.

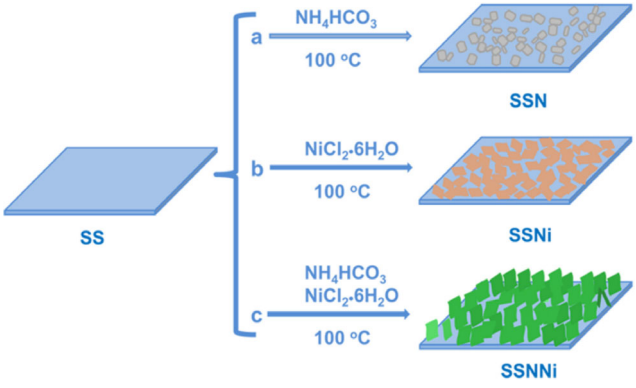

Figure 1 Schematic image of fabrication process of SSNNi.

3 Results and discussions

The morphology of the 3D SSNNi electrode was characterized using scanning electron microscopy (SEM). As shown in Figs. 1(a) and 1(b), compared to the smooth surface of SS, the surface of SSN is unevenly covered with spindle-like Ni(Fe) hydroxides particles, with an average size of 125 nm. These structures were formed owing to NH_4HCO_3, indicating the successful construction of Ni(Fe) hydroxides on SS, which is also confirmed by the X-ray diffraction (XRD) pattern (Fig. S1 in the Electronic Supplementary Material (ESM)). However, by importing only a small amount of extra Ni salts, closely packed Ni(Fe) hydroxide nanosheets form. These sheets were typically 200 nm in length and less than 15 nm in thickness, as confirmed in the SEM image of SSNi (Fig. 1(c)). This is more beneficial for electron and mass transport when compared with SSN. Furthermore, by simultaneously importing NH_4HCO_3 and extra Ni salts, dense films forming a 3D cross-linked nanosheet array (400 nm in length and less than 18 nm in thickness) appear, which are also favorable for enhancing the OER performance [24]. It is worth noting that NH_4HCO_3 plays a significant role in forming 3D vertical interconnected nanosheet arrays. When the amount of NH_4HCO_3 is reduced, the surfaces of SSNNi become packed with a 3D network containing only sparse vertical nanosheets and crisscrossed nanowires (Fig. S2(a) in the ESM). These interconnected nanowires can be assembled into a nanosheet by increasing the amount of NH_4HCO_3 (Fig. S2(b) in the ESM). However, excessive amounts of NH_4HCO_3 result in the disappearance of the nanosheet due to dissolution of the hydroxides. Moreover, when the anion is changed to OH^-, a vertical and less dense nanosheet network is obtained (Fig. S3(b) in the ESM), highlighting the importance of NH_4^+. Conversely, much thicker and larger nanosheets are tiled on the surface of SSNNi when the cation is replaced by Na^+ (Fig. S3(a) in the ESM). Interestingly, only 3D networks of nanowires are observed with the addition of NaOH instead of NH_4HCO_3 (Fig. S3(c) in the ESM). Therefore, both NH_4^+ and HCO_3^- are key factors in building the 3D cross-linked nanosheet arrays.

Energy dispersive spectroscopy–transmission electron microscopy (EDS–TEM) was performed to confirm the observed elemental distribution of the nanosheets on the SSNNi (Figs. 2(a)–2(e)). As shown in the element mapping images of the nanosheet for SSNNi, Ni, Fe, Cr, and O, they are found to be homogeneously overlapped throughout the nanosheet structure, suggesting the presence of a Ni(Fe) hydroxide nanosheet. To further elucidate the chemical structure of the dense film, X-ray photoelectron spectroscopy (XPS) was performed. The XPS survey spectra (Fig. 3 and Figs. S4–S6 in the ESM) suggest that Fe, Ni, Cr, and O are all present in the thin films of SSNNi. Moreover, the Ni content increases with the addition of Ni salts, accompanied by a decrease in the Fe content, indicating that the surface of SSNNi mainly consists of Ni hydroxide with trace Fe doping. Fortunately, as previously reported in the literature, Fe doping can increase the conductivity of NiOOH,

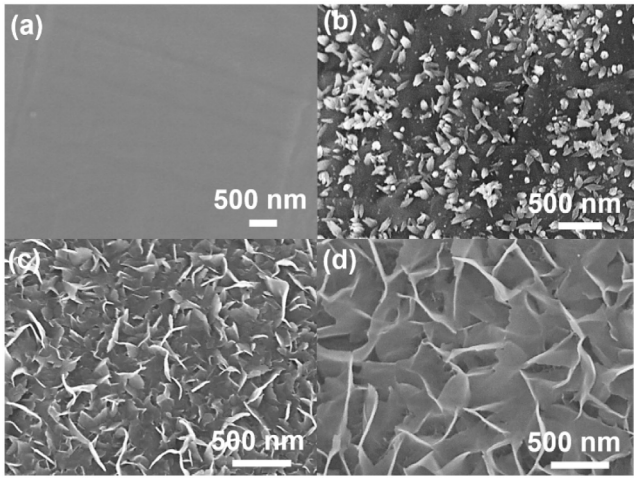

Figure 2 SEM images of SS (a), SSN (b), SSNi (c) and SSNNi (d).

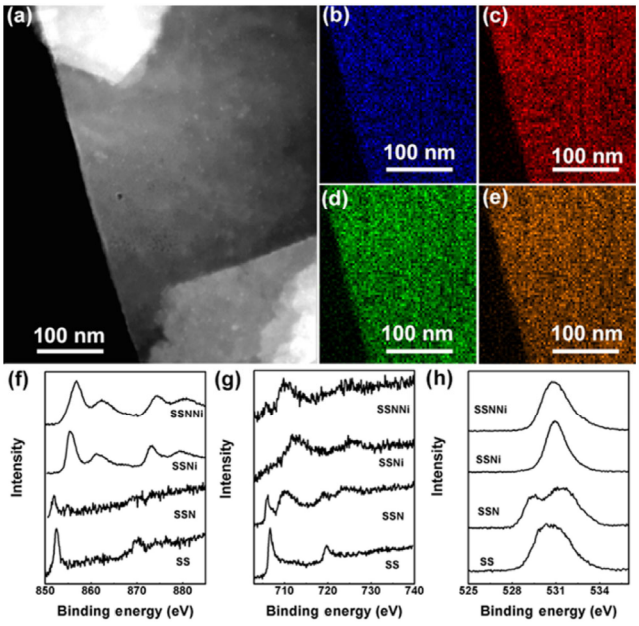

Figure 3 (a) High-angle annular dark-field scanning TEM (HDAAF-STEM) images of the nanosheet on the SSNNi electrode; the corresponding element mapping images of Fe (b), Ni (c), Cr (d) and O (e); high resolution Ni 2p (f), Fe 2p (g) and O 1s (h) XPS spectra of SS, SSN, SSNi and SSNNi.

which is necessary for catalyzing the OER [32]. In addition, the two spin–orbit doublets of the Ni 2p spectra for these electrodes are clearly observed, which belong to Ni^{3+} (Fig. 3(f) and Fig. S6(b) in the ESM) [33]. With respect to the Fe 2p spectra, the main two spin–orbit doublets in the spectrum correspond to Fe^{2+} and Fe^{3+} (Fig. 3(g) and Fig. S6(a) in the ESM) [34]. Additionally, the O1s spectrum indicates the presences of hydrophilic functional groups (OH^-, O^{2-}), which are beneficial for the penetration of the electrolyte (Fig. 3(h)) [22]. Thus, it is clear that the nanosheet mainly consists of Ni(Fe)O_xH_y, which may be active sites for the OER.

The electrocatalytic activity of the SSNNi electrode was investigated in a standard three-electrode electrochemical cell in an alkaline electrolyte. The SSNNi was directly used as a working electrode, while a saturated calomel electrode (SCE) and Pt mesh served as the reference electrode and counter electrode, respectively. The potentials were converted to the reversible hydrogen electrode (RHE) reference by calibration.

As displayed in Fig. 4(a), the SSN requires lower overpotential (0.31 V at 20 mA·cm^{-2}) and greater current density compared to the bare SS. This is likely due to the removal of anticorrosive species and the growth of Ni(Fe) hydroxide particles on the SSN. To further increase the amount of active species for OER, a small quantity of extra Ni salts was introduced to compensate for the relatively low content of Ni in stainless steel. As expected, although NH_4HCO_3 is absent, higher OER performance of SSNi with lower overpotential (0.28 V at 20 mA·cm^{-2}) was achieved compared to SSN. The superior OER performance can be ascribed to the nanosheet tiled on the surface of SSNi electrode, and enhanced mass and electron transport. Furthermore, SSNNi, possessing 3D crisscrossed nanosheet arrays, captures even better OER overpotential (0.23 V) at the same current density, compared to SSNi, SSN, and SS. This can be attributed to more accessible active sites, intimate connection between the active species and the current collector, and better electron and mass transport. To gain deeper insight into the OER activity, the Tafel slope of these electrodes were investigated. As shown in Fig. 4(b), the resulting Tafel slope of SSNNi is 36 mV·dec^{-1}, smaller than those of SSNi (37 mV·dec^{-1}), SSN (38 mV·dec^{-1}), and SS (68 mV·dec^{-1}), and also superior to the previously reported Fe–Ni OER catalysts. The SSNNi even outperformed the RuO_2 (62 mV·dec^{-1}) and the Ir/C (120 mV·dec^{-1}) catalysts, suggesting faster OER kinetics (Fig. 4(b) and Figs. S7 and S8, Table S2 in the ESM) [3, 6, 35]. Electrochemical impedance spectroscopy (EIS) was applied to obtain further insight into the charge-transfer kinetics of the OER process. As shown in Fig. 4(c), lower charge-transfer resistance was observed for SSNNi compared to SSNi, suggesting that the 3D nanosheet array is more favorable for electron transport than the 2D tiled nanosheet. Additionally, although the dense nanosheets on the surfaces of SSNNi and SSNi result in slightly larger resistances in comparison with SSN and SS, they still possess higher OER performance. This is because the OER performance is determined by many factors, such as conductivity, mass transport, active site abundance, among others. Moreover, the electrochemical double layer capacitance (C_{dl}) [36] was investigated to evaluate the electrochemical active surface area (ECSA) of the as-prepared samples. As shown in Fig. S9 and Table S1 in the ESM, SSNNi has

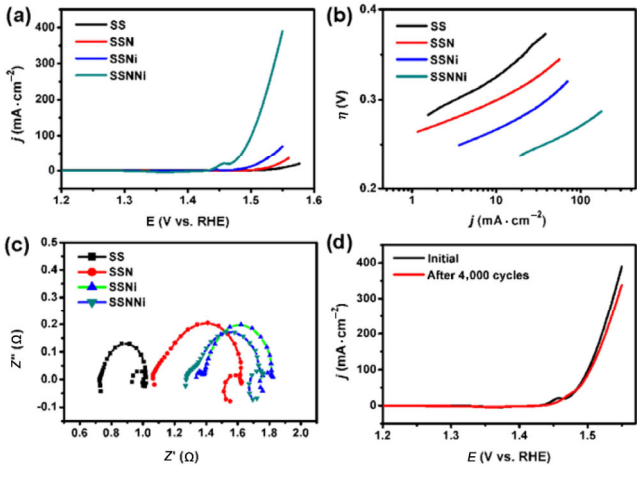

Figure 4 OER polarization curves (a), Tafel plots (b) and EIS (c) of SS, SSN, SSNi and SSNNi; (d) OER polarization curves of SSNNi before and after 4,000 potential cycles.

the larger C_{dl} compared with the control samples, indicating its larger ECSA, which contributes to its higher OER catalytic activity. Thus, the SSNNi with larger ECSA has more active sites and yields a higher OER catalytic performance.

As the stability of the electrode for OER is also important for practical energy conversion systems, continuous potential cycling was performed to probe the durability of the SSNNi electrode. As shown in Fig. 4(d), the SSNNi exhibits long-term stability with only slight anode current attenuation (less than 7%) after operating with 4,000 continuous potential cycles in the alkaline electrolyte. This excellent stability may be due to the stable 3D structure that remained static with respect to morphology, and prevented the accumulation of gases (Fig. S10 in the ESM). Note that no Fe/Ni was detected in the electrolyte by inductively coupled plasma-atomic emission spectroscopy (ICP-AES), further indicating its stability. Therefore, the high OER catalytic activity of SSNNi, which includes low OER overpotential, small Tafel slope, large current density, and long-term durability makes it a highly promising candidate to replace noble metal based OER catalysts.

4 Conclusions

In conclusion, a facile and scalable design was proposed to synthesize a hierarchical 3D crisscrossed nanosheet array on a stainless steel mesh. The SS described here is not only used as the current collector, but also as the source of generated Ni(Fe) based active materials. NH_4HCO_3 also plays vital role in the formation of the 3D nanosheet array. The resultant SSNNi, featuring a well-defined 3D interconnected nanosheet array with more exposed and accessible active sites, improved electron and mass transport, and stable structure yields excellent OER performance. The high performance of SSNNi was indicated by low overpotential, fast kinetics (small Tafel slope), large current density, and long-term durability. Moreover, this 3D integrated OER electrode is suited for large-scale fabrication, and can be adapted for the fabrication of similar 3D electrodes for other applications, such as Li-ion batteries and supercapacitors.

Acknowledgements

This work is financially supported by the National Natural Science Foundation of China (Nos. 51472209, U1401241, 51522101, 51471075, 5163100, and 51401084), and Specialized Research Fund for the Doctoral Program of Higher Education of China (No. 20110061120040).

Electronic Supplementary Material: Supplementary material (further details of the prepared procedures, SEM measurements, XRD spectra and XPS spectroscopy measurements) is available in the online version of this article at https://doi.org/10.1007/s12274-017-1743-8.

References

[1] Chow, J.; Kopp, R. J.; Portney, P. R. Energy resources and global development. *Science* **2003**, *302*, 1528–1531.

[2] Wu, J.; Xue, Y.; Yan, X.; Yan, W. S.; Cheng, Q. M.; Xie, Y. Co_3O_4 nanocrystals on single-walled carbon nanotubes as a highly efficient oxygen-evolving catalyst. *Nano Res.* **2012**, *5*, 521–530.

[3] Wang, J.; Li, K.; Zhong, H. X.; Xu, D.; Wang, Z. L.; Jiang, Z.; Wu, Z. J.; Zhang, X. B. Synergistic effect between metal–nitrogen–carbon sheets and NiO nanoparticles for enhanced electrochemical water-oxidation performance. *Angew. Chem., Int. Ed.* **2015**, *54*, 10530–10534.

[4] Gong, M.; Dai, H. J. A mini review of NiFe-based materials as highly active oxygen evolution reaction electrocatalysts.

Nano Res. **2015**, *8*, 23–39.

[5] Tüysüz, H.; Hwang, Y. J.; Khan, S. B.; Asiri, A. M.; Yang, P. D. Mesoporous Co_3O_4 as an electrocatalyst for water oxidation. *Nano Res*. **2013**, *6*, 47–54.

[6] Liu, Q. C.; Jiang, Y. S.; Xu, J. J.; Xu, D.; Chang, Z. W.; Yin, Y. B.; Liu, W. Q.; Zhang, X. B. Hierarchical Co_3O_4 porous nanowires as an efficient bifunctional cathode catalyst for long life Li–O_2 batteries. *Nano Res*. **2015**, *8*, 576–583.

[7] Peng, Z.; Jia, D. S.; Al-Enizi, A. M.; Elzatahry, A. A.; Zheng, G. F. From water oxidation to reduction: Homologous Ni–Co based nanowires as complementary water splitting electrocatalysts. *Adv*. *Energy Mater*. **2015**, *5*, 1402031.

[8] Cobo, S.; Heidkamp, J.; Jacques, P. A.; Fize, J.; Fourmond, V.; Guetaz, L.; Jousselme, B.; Ivanova, V.; Dau, H.; Palacin, S. et al. A Janus cobalt-based catalytic material for electro-splitting of water. *Nat*. *Mater*. **2012**, *11*, 802–807.

[9] Wang, L. X.; Geng, J.; Wang, W. H.; Yuan, C.; Kuai, L.; Geng, B. Y. Facile synthesis of Fe/Ni bimetallic oxide solid-solution nanoparticles with superior electrocatalytic activity for oxygen evolution reaction. *Nano Res*. **2015**, *8*, 3815–3822.

[10] Hardin, W. G.; Mefford, J. T.; Slanac, D. A.; Patel, B. B.; Wang, X. Q.; Dai, S.; Zhao, X.; Ruoff, R. S.; Johnston, K. P.; Stevenson, K. J. Tuning the electrocatalytic activity of perovskites through active site variation and support interactions. *J*. *Chem*. *Mater*. **2014**, *26*, 3368–3376.

[11] Zhu, Y. L.; Zhou, W.; Chen, Z. G.; Chen, Y. B.; Su, C.; Tadé, M. O.; Shao, Z. P. $SrNb_{0.1}Co_{0.7}Fe_{0.2}O_{3-\delta}$ perovskite as a next-generation electrocatalyst for oxygen evolution in alkaline solution. *Angew*. *Chem*., *Int*. *Ed*. **2015**, *54*, 3897–3901.

[12] Chang, J. F.; Xiao, Y.; Xiao, M. L.; Ge, J. J.; Liu, C. P.; Xing, W. Surface oxidized cobalt-phosphide nanorods as an advanced oxygen evolution catalyst in alkaline solution. *ACS Catal*. **2015**, *5*, 6874–6878.

[13] Liu, X. J.; Chang, Z.; Luo, L.; Xu, T. H.; Lei, X. D.; Liu, J. F.; Sun, X. M. Hierarchical $Zn_xCo_{3-x}O_4$ nanoarrays with high activity for electrocatalytic oxygen evolution. *Chem*. *Mater*. **2014**, *26*, 1889–1895.

[14] Gong, M.; Li, Y. G.; Wang, H. L.; Liang, Y. Y.; Wu, J. Z.; Zhou, J. G.; Wang, J.; Regier, T.; Wei, F.; Dai, H. J. An advanced Ni–Fe layered double hydroxide electrocatalyst for water oxidation. *J*. *Am*. *Chem*. *Soc*. **2013**, *135*, 8452–8455.

[15] Huang, J. H.; Chen, J. T.; Yao, T.; He, J. F.; Jiang, S.; Sun, Z. H.; Liu, Q. H.; Cheng, W. R.; Hu, F. C.; Jiang, Y. et al. CoOOH nanosheets with high mass activity for water oxidation. *Angew*. *Chem*., *Int*. *Ed*. **201**5, *54*, 8722–8727.

[16] Jin, H. Y.; Wang, J.; Su, D. F.; Wei, Z. Z.; Pang Z. F.; Wang, Y. *In situ* cobalt-cobalt oxide/N-doped carbon hybrids as superior bifunctional electrocatalysts for hydrogen and oxygen evolution. *J*. *Am*. *Chem*. *Soc*. **2015**, *137*, 2688–2694.

[17] Li, Y.; Zhang, L. H.; Liu, R. R.; Cao, Z.; Sun, X. M.; Liu, X. J.; Luo, J. Wo_3@α-Fe_2O_3 heterojunction arrays with improved photoelectrochemical behavior for neutral pH water splitting. *ChemCatChem* **2016**, *8*, 2765–2770.

[18] Wang, J. H.; Cui, W.; Liu, Q.; Xing, Z. C.; Asiri, A. M.; Sun, X. P. Recent progress in cobalt-based heterogeneous catalysts for electrochemical water splitting. *Adv*. *Mater*. **2016**, *28*, 215–230.

[19] Wang, Y.; Ding, W.; Chen, S. G.; Nie, Y.; Xiong, K.; Wei, Z. D. Cobalt carbonate hydroxide/C: An efficient dual electrocatalyst for oxygen reduction/evolution reactions. *Chem*. *Commun*. **2014**, *50*, 15529–15532.

[20] Zhang, C.; Antonietti, M.; Fellinger, T. P. Blood ties: Co_3O_4 decorated blood derived carbon as a superior bifunctional electrocatalyst. *Adv*. *Funct*. *Mater*. **2014**, *24*, 7655–7665.

[21] Zhao, A. Q.; Masa, J.; Xia, W.; Maljusch, A.; Willinger, M. G.; Clavel, G.; Xie, K. P.; Schlögl, R.; Schuhmann, W.; Muhler, M. Spinel Mn-Co oxide in N-doped carbon nanotubes as a bifunctional electrocatalyst synthesized by oxidative cutting. *J*. *Am*. *Chem*. *Soc*. **2014**, *136*, 7551–7554.

[22] Chen, S.; Duan, J. J.; Jaroniec, M.; Qiao, S. Z. Three-dimensional N-doped graphene hydrogel/NiCo double hydroxide electrocatalysts for highly efficient oxygen evolution. *Angew*. *Chem*., *Int*. *Ed*. **2013**, *52*, 13567–13570.

[23] Ma, T. Y.; Cao, J. L.; Jaroniec, M.; Qiao, S. Z. Interacting carbon nitride and titanium carbide nanosheets for high-performance oxygen evolution. *Angew*. *Chem*., *Int*. *Ed*. **2016**, *55*, 1138–1142.

[24] Chen, P. Z.; Xu, K.; Fang, Z. W.; Tong, Y.; Wu, J. C.; Lu, X. L.; Peng, X.; Ding, H.; Wu, C. Z.; Xie, Y. Metallic Co_4N porous nanowire arrays activated by surface oxidation as electrocatalysts for the oxygen evolution reaction. *Angew*. *Chem*., *Int*. *Ed*. **2015**, *54*, 14710–14714.

[25] Wang, J.; Zhong, H. X.; Qin Y. L.; Zhang, X. B. An efficient three-dimensional oxygen evolution electrode. *Angew*. *Chem*., *Int*. *Ed*. **2013**, *52*, 5248–5253.

[26] Haber, J. A.; Cai, Y.; Jung, S.; Xiang, C. X.; Mitrovic, S.; Jin, J.; Bell, A. T.; Gregoire, J. M. Discovering Ce-rich oxygen evolution catalysts, from high throughput screening to water electrolysis. *Energy Environ*. *Sci*. **2014**, *7*, 682–688.

[27] Lu, X. Y.; Zhao, C. Electrodeposition of hierarchically structured three-dimensional nickel–iron electrodes for efficient oxygen evolution at high current densities. *Nat*. *Commun*. **2015**, *6*, 6616.

[28] Schäfer, H.; Beladi-Mousavi, S. M.; Walder, L.; Wollschläger, J.; Kuschel, O.; Ichilmann, S.; Sadaf, S.; Steinhart, M.; Küpper, K.; Schneider, L. Surface oxidation of stainless steel: Oxygen evolution electrocatalysts with high catalytic activity. *ACS Catal*. **2015**, *5*, 2671–2680.

[29] Schäfer, H.; Sadaf, S.; Walder, L.; Kuepper, K.; Dinklage, S.; Wollschläger, J.; Schneider, L.; Steinhart, M.; Hardege J.; Daum, D. Stainless steel made to rust: A robust water-splitting catalyst with benchmark characteristics. *Energy Environ. Sci.* **2015**, *8*, 2685–2697.

[30] Tang, C.; Cheng, N. Y.; Pu, Z. H.; Xing, W.; Sun, X. P. NiSe nanowire film supported on nickel foam: An efficient and stable 3D bifunctional electrode for full water splitting. *Angew. Chem., Int. Ed.* **2015**, *54*, 9351–9355.

[31] Batchellor, A. S.; Boettcher, S. W. Pulse-electrodeposited Ni–Fe (oxy)hydroxide oxygen evolution electrocatalysts with high geometric and intrinsic activities at large mass loadings. *ACS Catal.* **2015**, *5*, 6680–6689.

[32] Burke, M. S.; Enman, L. J.; Batchellor, A. S.; Zou, S. H.; Boettcher, S. W. Oxygen evolution reaction electrocatalysis on transition metal oxides and (oxy) hydroxides: Activity trends and design principles. *Chem. Mater.* **2015**, *27*, 7549–7558.

[33] Liang, H. F.; Meng, F.; Cabán-Acevedo, M.; Li, L. S.; Forticaux, A.; Xiu, L. C.; Wang, Z. C.; Jin, S. Hydrothermal continuous flow synthesis and exfoliation of NiCo layered double hydroxide nanosheets for enhanced oxygen evolution catalysis. *Nano Lett.* **2015**, *15*, 1421–1427.

[34] Biesinger, M. C.; Payne, B. P.; Grosvenor, A. P.; Lau, L. W. M.; Gerson, A. R.; Smart, R. S. C. Resolving surface chemical states in XPS analysis of first row transition metals, oxides and hydroxides: Cr, Mn, Fe, Co and Ni. *Appl. Surf. Sci.* **2011**, *257*, 2717–2730.

[35] Liu, Y. W.; Cheng, H.; Lyu, M.; Fan, S. J.; Liu, Q. H.; Zhang, W. S.; Zhi, Y. D.; Wang, C. M.; Xiao, C.; Wei, S. Q. et al. Low overpotential in vacancy-rich ultrathin $CoSe_2$ nanosheets for water oxidation. *J. Am. Chem. Soc.* **2014**, *136*, 15670–15675.

[36] Leng, M.; Huang, X. L.; Xiao, W.; Ding, J.; Liu, B. H.; Du, Y. H.; Xue, J. M. Enhanced oxygen evolution reaction by Co-O-C bonds in rationally designed Co_3O_4/graphene nanocomposites. *Nano Energy* **2017**, *33*, 445–452.